Available online at www.sciencedirect.com

ScienceDirect

Energy Procedia 69 (2015) 790 – 801

Energy Procedia

International Conference on Concentrating Solar Power and Chemical Energy Systems, SolarPACES 2014

Simulation of flux distributions on the foam absorber with solar reactor for thermo-chemical two-step water splitting H_2 production cycle by the 45 kW_{th} KIER solar furnace

H.S. Cho[a†], N. Gokon[b], T. Kodama[c]
Y.H. Kang[d], J.K. Kim[d]

[a]*Graduate school of Science and Technology, University, 8050 Ikarashi 2-nocho, Nishi-ku, Niigata 950-2181, JAPAN*
[b] *Center for Transdisciplinary Research, Niigata University, 8050 Ikarashi 2-nocho, Nishi-ku, Niigata 950-2181, JAPAN*
[c]*Dep. of Chemistry & Chemical Engineering, Faculty of Engineering, Niigata University, 8050 Ikarashi 2-nocho, Nishi-ku, Niigata 950-2181, JAPAN*
[c]*Department of Solar energy, Korea Institute of Energy Research, Yuseong go, Daejeon, 304-343, KOREA*

Abstract

The flux distributions on the device in the solar reactor with the solar furnace were studied. This study aims to understand of characters of concentrated sun rays through KIER solar furnace and design of device shape for uniform heat distribution on the device surface. For the calculation of heat flux on the device with the KIER solar furnace, the optical modeling program Soltrace was used. At first, the KIER 45 kW_{th} solar furnace and flat disk type device shape was simulated for understand of past experimental results. And then 3 cylinder shape device model and 1 conical shape device model was suggested and the heat flux intensity on the device was calculated. Finally, 5 models which is including flat disk type device shape, 3 cylinder shape, and 1 conical shape device models was calculated and compared. The results show that the concentrated sun rays from dish and heat flux intensity are has a directional characteristic concentrated to normal direction than perpendicular direction. The results will be applied to next solar demonstrations which are design of new solar reactor and new device shape.

© 2015 The Authors. Published by Elsevier Ltd. This is an open access article under the CC BY-NC-ND license (http://creativecommons.org/licenses/by-nc-nd/4.0/).
Peer review by the scientific conference committee of SolarPACES 2014 under responsibility of PSE AG

Keywords: Foam device, Two-step water splitting, Solar reactor, Solar furnace, Heat flux

1876-6102 © 2015 The Authors. Published by Elsevier Ltd. This is an open access article under the CC BY-NC-ND license (http://creativecommons.org/licenses/by-nc-nd/4.0/).
Peer review by the scientific conference committee of SolarPACES 2014 under responsibility of PSE AG
doi:10.1016/j.egypro.2015.03.088

1. Introduction

Concentrated solar radiation is used as the energy source for high temperature process heat to drive chemical reactions towards the production of storable and transportable fuels. Various solar chemical receiver/absorbers or reactors with redox materials has been proposed, developed and tested for realizing hydrogen production using a concentrated solar radiation [1]. The concept of using metal oxides as substrate for thermochemical production of hydrogen was suggested by Nakamura (1977), in which cycling between Fe_3O_4 and FeO was demonstrated [2]. Among the variety of metal oxides, ceria has emerged as an attractive redox material due to its ability to rapid conduct oxygen contributing to fast redox kinetics, as compared to ferrite-based metal oxides [1].

The two step water splitting cycle based on nonstoichiometric ceria is represented by following equations.

$$CeO_2 \rightarrow CeO_{2-\delta} + 1/2\delta O_2 \quad (1)$$

$$CeO_{2-\delta} + \delta H_2O \rightarrow CeO_2 + \delta H_2 \quad (2)$$

The first step (Thermal reduction) is highly endothermic (ΔH = 198 kJ/mol CeO_2 at 2300 K) and heat is supplied by concentrated solar radiation and oxygen is released. In the reduction step, ceria is thermally reduced to a nonstoichiometric state in which it can react with steam. The second step (Water decomposition) is exothermic (ΔH = − 125 kJ/mol at 700 K), in which case hydrogen is produced [3-5]. Several studies examined the suitability of ceria for thermochemical fuel production, applying thermochemical study and CO_2/H_2O splitting with the reticulated pure ceria [6].

Niigata University has developed ceramic foam devices whose foam matrix is made of MgO-partially stabilized zirconia (MPSZ). The MPSZ foam matrix has superior characteristics as compared with SiSiC and SiC[7], including high heat resistance and chemical inertness with iron oxide at high temperature. Also, the foam structure can effectively absorb light irradiation owing to its specifically large surface area. These foam devices were possible for multi-cycling the two-step water splitting process [8-11]. Niigata University started an international project for solar two-step water splitting cycle using a foam device reactor: a joint research project between Niigata University (Japan) and Korea Institute of Energy Research (Korea) started in 2012. The reactive water splitting foam device was developed and prepared by Niigata University, and involves coating zirconia foam with ceria [12]. The objectives of the project are to develop reactive foam devices with ceria as the working material, to design and fabricate a solar reactor with the reactive foam device, and finally, to demonstrate its performance in sunlight with a KIER 45 kW_{th} solar furnace. From 2012 to 2013, the thermochemical two-step water splitting cycle which use a ceria coated ceramic foam device as a redox material for hydrogen production with a 45kW_{th} solar furnace, have been validated by the hydrogen production.

However, due to the ceria coated foam device having a disk shape, the distribution of heat flux on the device was non-uniform. It was verified by photographs captured by the CCD camera during the experiment. Figure 1 shows the photograph of device surface at the thermal reduction step, in which is seen, significantly, the release of oxygen at the center, not the side-activated are. The feature point of CeO_2 material is the discoloration phenomenon between reduced phase and the oxidized phase. The reduced phase of CeO_2 shows a darker color than in the original state. In fact, the flux distribution in the solar reactor (or on the device surface) has a direct effect on the efficiency of hydrogen production. The radiation flux distribution in the solar reactor depended on directional distribution and quantity of concentrated energy in the focal region of solar concentrating system [13, 14].

Fig 1. A photograph of ceria coated foam device under the thermal reduction step

The objectives of the this research is to design reactive ceramic foam device shapes to obtain uniform flux distribution on the device for the purpose of increasing the hydrogen production efficiency with solar furnace system.

By the use of the code SolTrace (NREL, National Renewable Energy Laboratory, USA), an optical design program of solar concentrating systems, the KIER 45kW$_{th}$ solar furnace system was simulated, after which several device shape models were studied in turn.

2. Simulation of KIER 45 kW$_{th}$ solar furnace by SolTrace

2.1 Introduction of SolTrace program

The SolTrace code is based on Monte Carlo ray tracing methodology for accurate representation of these varied and complex systems. SolTrace is one of several options available for modeling CSP systems. Since its inception, similar tools have been developed by others in the CSP community, such as Tonatiuh. In addition, commercial ray-tracing packages also exist, such as ASAP by Breault Research, but these are intended for more general optical system design and, as such, are not "solar friendly." While they can be used, they require significant effort to learn and model the complex solar designs using the sun as the source. The code utilizes a ray-tracing methodology of Monte-carlo method. A specified number of rays are traced from the sun through the system, and each traces through the defined system while encountering various optical interactions. Such a code has the advantage over codes based on convolution of moments in that it replicates real photon interactions and can therefore provide accurate results for complex systems that cannot be modeled otherwise. Accuracy increases with the number of rays traced, and larger ray numbers means more processing time. Complex geometries also translate into longer run times. However, the required number of rays is also a function of the desired result [15].

2.2 Simulation of KIER 45 kW$_{th}$ solar furnace system with flat disk type foam device (or foam absorber)

Figure 2 and Table 1 shows a photograph and specifications of 45kW$_{th}$ KIER solar furnace system. The solar furnace system was installed in KIER(Korea Institute of Energy Reseach), Korea. The area of heliostat and parabolic reflector are 87.35 m^2 and 61.82 m^2, focal length is 4.98 m [16]. Heliostat consists of small pieces of flat type mirror and the reflectivity of the mirror is 0.80 around. Parabolic reflector consists of 144 curved shape mirrors and the reflectivity is 0.91 around. The rim angle of the parabolic reflector is 48°. The thermal capacity of the system is about 45 kW thermal and the maximum concentraion ratio is 5050 suns. KIER solar furnace system includes the blind and shutter for the control of the intensity reflected solar radiation [17,18].

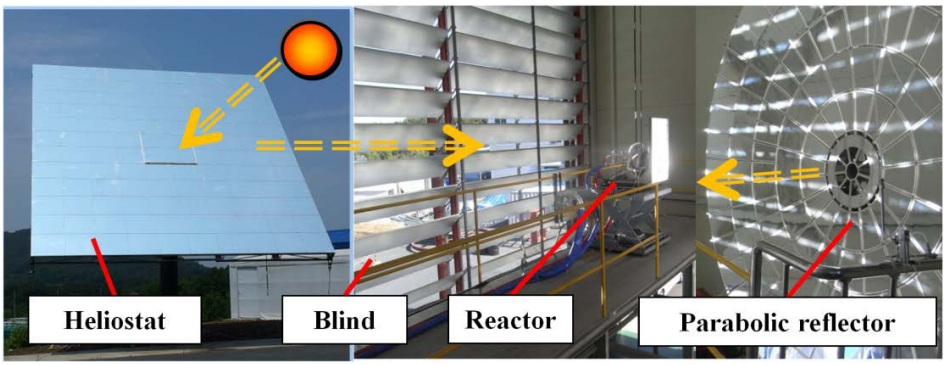

Fig 2. A photograph of KIER 45kW$_{th}$ Solar furnace system

Table 1. Specification of 45 kW_{th} KIER solar furnace system

Heliostat area (m^2)	Parabolic mirror area (m^2)	Distance from two reflector (m)	Focus length (m)	Rim angle (°)
87.35	61.82	35	4.98	48

Figure 3 shows the geometry of simulated KIER 45kW_{th} solar furnace system with solar reactor involving the flat disk type foam device (represented to "foam absorber" from followings). The solar reactor equipped transparent quartz window to pass concentrated solar radiation for directly heating a redox material coated foam absorber. Figure 4, 5 shows the schematic and photograph of the solar reactor and simulated parts. The insulation board at the front of solar reactor, flange parts of solar reactor at the aperture, and the quartz window (267 mm) were included in the simulation. The inner wall surface of solar reactor main body, covered by Inconel steel sheet, was also considered.

The simulated sun position was assumed to fix to top of heliostat, and the sun shape was used to CSR5 – offered from the SolTrace in which parameter defining a Gaussian distribution for the suns' disk. In terms of slope error from the heliostat and parabolic reflector (dish) were set to 2 mrad by initial value of SolTrace.

The flat disk type foam absorber shape was simulated to understand implemented data from experiments in 2012 and 2013. The diameter of the flat type foam absorber is 15 cm, and thickness is 3 cm. During the experiment (from 2012 to 2013), the flat type foam absorber laid on – 8cm back side from the focal point of solar furnace. Its aim was to expand the uniform heat flux on the foam absorber. According to the results of the experiments, it did not actually show uniform heat flux distribution.

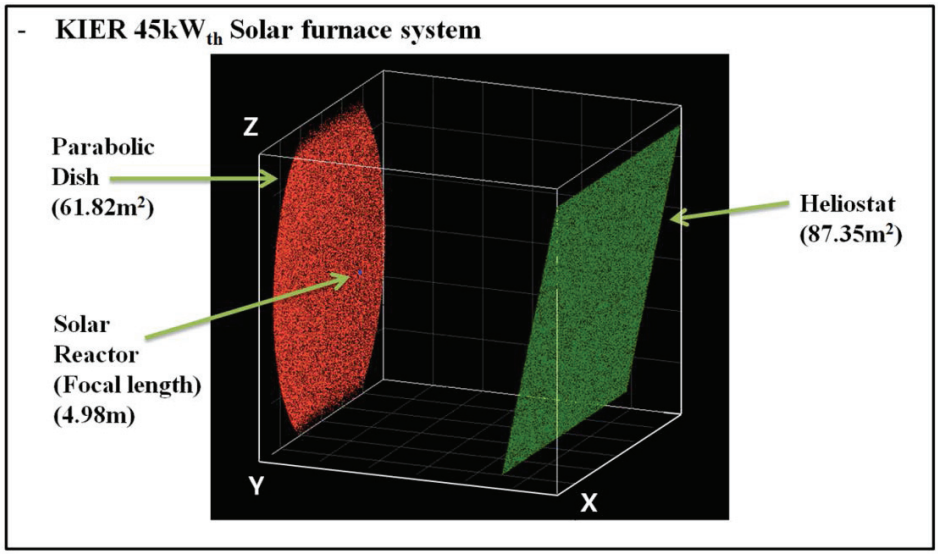

Fig 3. Result of simulated KIER 45kW_{th} Solar furnace system by the SolTrace code

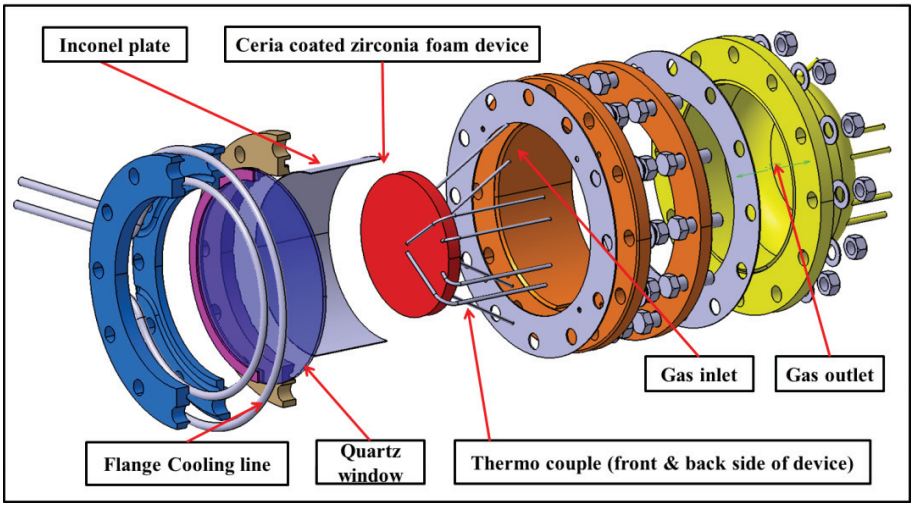

Fig 4. Schematic of solar reactor and flat type foam absorber

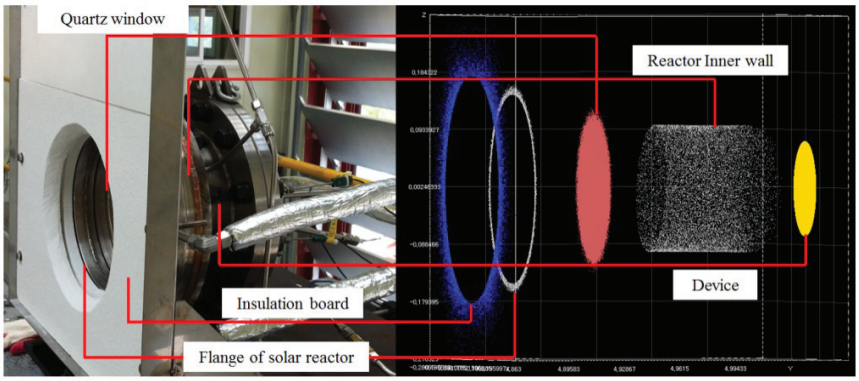

Fig 5. A photograph of solar reactor and the simulated part of solar reactor for the consideration of rays blocking

3. Simulation of flux distribution on the devices

3.1 Design of foam absorber shape – 5 models

The design of the foam absorber shape aims at a uniform flux distribution over the foam absorber surface and an increase in the surface area by which is direct incident lights arrives. The first idea of the device shape was based on cavity shape, as for instance, cylinder structures and conical shapes. The simulation on flux distribution was studied using 5 models – the flat type, 4 cylinder shapes, and 1 conical shape. Each model has a different aperture size, diameters, thickness, and volume.

Figure 6, and Table 2 show comparisons and properties of the 5 models. In Table 2, the direct exposure area (as shown fig. 6 by yellow lines) ratio and volume ratio was compared with that of the flat disk device.

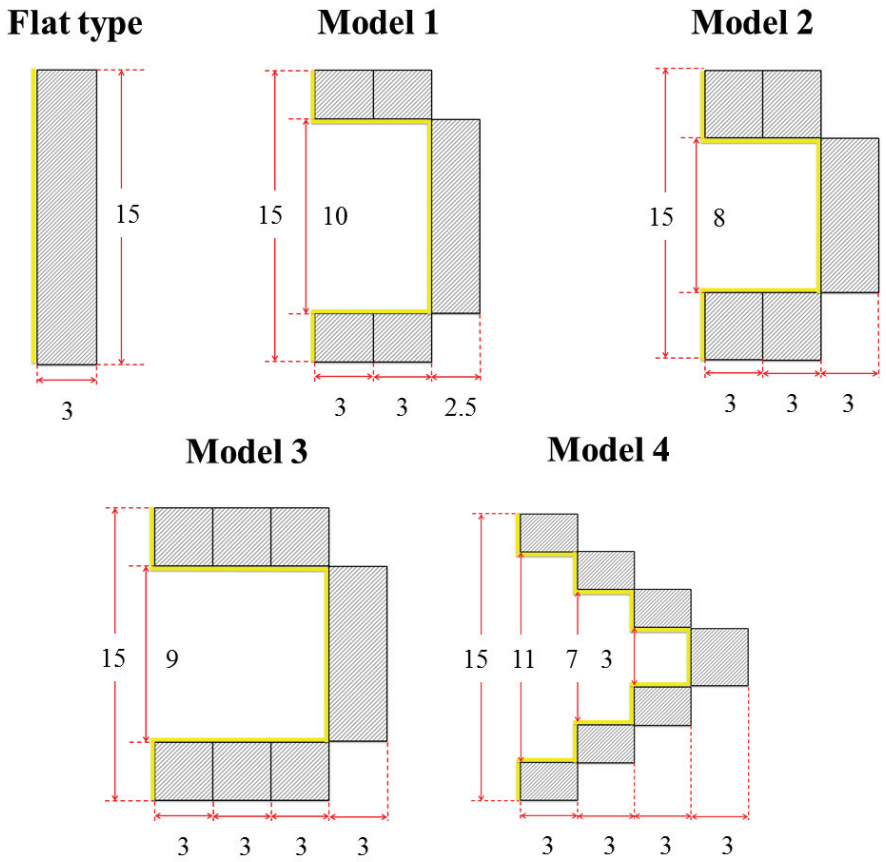

Fig 6. Design of foam absorbers – flat type, 4 cylinders shape, 1 conical shape (model 4 assumed to conical shapes) and the yellow lines show the area which direct exposure area.

Table 2. Comparison of the 5 models properties – direct exposure area, volume, ratios with flat type disk device

	Flat	Model 1	Model 2	Model 3	Model 4	Unit
Exposure Area	176.625	365.025	327.345	430.965	374.445	Cm^2
	0.0176625	0.0365025	0.0327345	0.0430965	0.0374445	m^2
Volume	529.875	785	909.03	1208.115	529.875	Cm^3
	0.000529875	0.000785	0.00090903	0.001208115	0.050889195	m^3
Area Ratio	1	2.07	1.85	2.44	2.12	None
Vol. Ratio	1	1.48	1.72	2.28	1	None

The outer diameter of models limited to 15cm – the same as flat disk type; the 4 cylinder model has an aperture size from 8cm to 10cm whereas the conical shape has an 11 cm. In the case of model 4, it has a stepwise structure exactly; however, it was named and assumed as a conical shape, having an aperture angle of 24 ^{o}.

The compared ratios show an increased exposure area and volume. The increased expose area (surface area) was expected to be a benefit, by absorbing the concentrated rays more than the flat disk type device could. And the increased volume has an advantage of larger volume for more coats of reactive materials. Model 3 shows the largest exposure area and volume due to having more depth than other models.

3.2 Basic comparison of 5 models and Boundary condition of simulation

A basic calculation of average heat flux intensity by the input power divide exposure area was studied. Based on the experimental data, the input power was decided with a range of 12 kW to 26 kW. Table 3. shows ideal heat flux intensity on the surface area of devices.

Table 3. Basic calculation of flux intensity – An ideal heat flux intensity on the exposure area divided from input power

Input power	Flat	Model 1	Model 2	Model 3	Model 4
	Input power / Direct exposure surface area				
kW	kW/m^2	kW/m^2	kW/m^2	kW/m^2	kW/m^2
12	679.41	328.74	366.59	278.44	320.47
14	792.64	383.54	427.68	324.85	373.89
16	905.87	438.33	488.78	371.26	427.30
18	1019.11	493.12	549.88	417.67	480.71
20	1132.34	547.91	610.98	464.07	534.12
22	1245.58	602.70	672.07	510.48	587.54
24	1358.81	657.49	733.17	556.89	640.95
26	1472.05	712.28	794.27	603.30	694.36

The basic calculations allow a comparison among 5 models. It can be utilized to decide the simulation condition for input power. For the simulation of heat flux distribution, the input power was 23 kW to 26 kW approximatively.

The boundary condition reflectivity of heliostat and dish are suggested from experimented data, approximating 0.89. And the absorptivity of foam absorber model was excluded due to following reason. The colour of foam absorber changed during the solar demonstration. Consequently, deciding the absorptivity was difficult, since the absorptivity relates to the colour of the foam absorber.

4. Results of simulation

4.1 Geometry of the 5 models from the simulation

The 5 suggested models were calculated and compared. Initially, the flat disk type was set on an -8cm position to form the focal points for the KIER solar furnace, in keeping with prior experimental conditions. However, in the other case, the device position was set on focal point of the KIER solar furnace. The focal point is 4.98 m from the mid-point of dish. The number of sun rays for calculation was 1,000,000 for obtaining higher accuracy calculation.

Figure 7. shows the geometries of simulated models that are represented by several dots. The dots signify the arrival of sun rays that are in turn reflected and concentrated from dish to surface of the device.

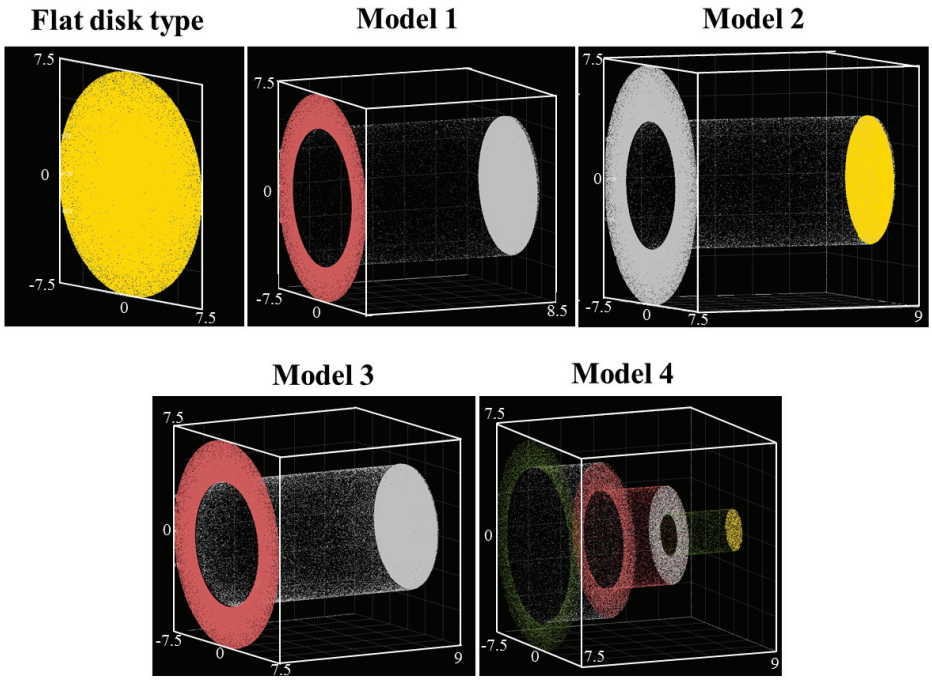

Fig 7. Simulated geometries – Flat disk type, 4 cylinders shape, 1 conical shape

4.2 Flux distributions of the 5 models

Figure 8. (a) ~ (e) shows the arrived heat flux contours and flux gradients of the 5 simulated models. Figure 8(a) shows the reflected sun rays and the result of the flat disk type. The heat flux contour and flux gradient was described with separated surfaces: the ring zone, the cylinder wall zone, and the flat disk zone. Figures 8.(b) ~ (e) were explained with an insisted arrow line. The cylinder wall zone was unrolled to draw a flux intensity contour.

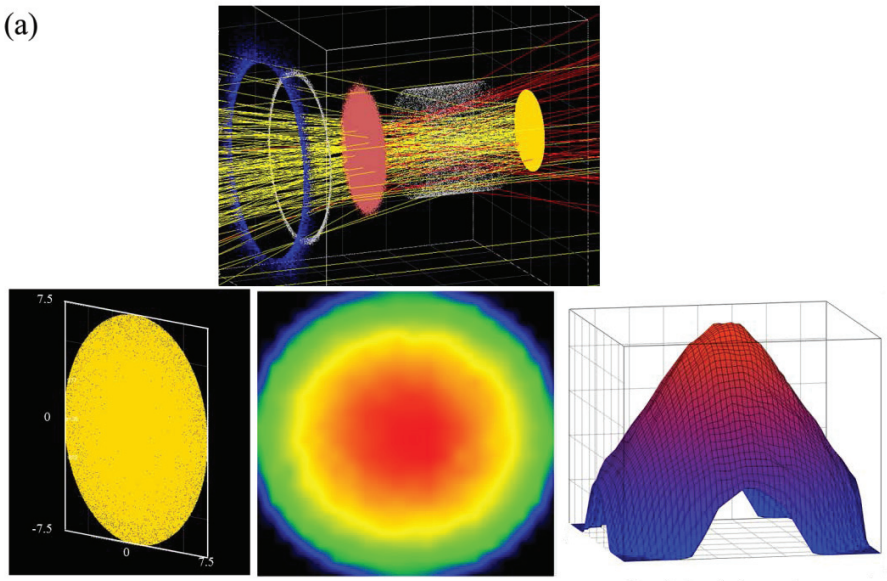

Fig 8 (a). Concentrated rays arriving to flat disk type device and the contour of flux intensity

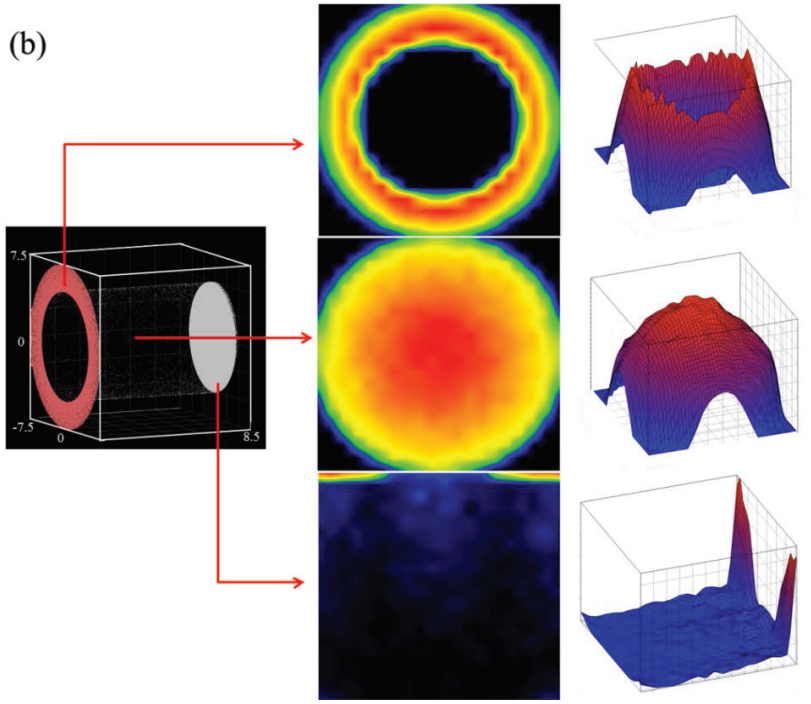
(b)
7.5
0
-7.5
0
8.5

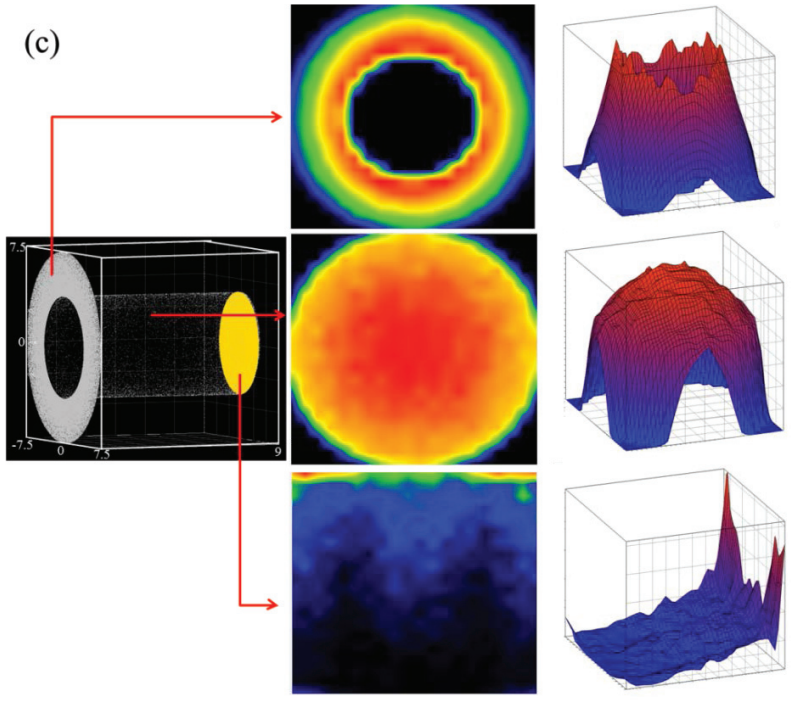
(c)
7.5
0
-7.5
0
7.5
9

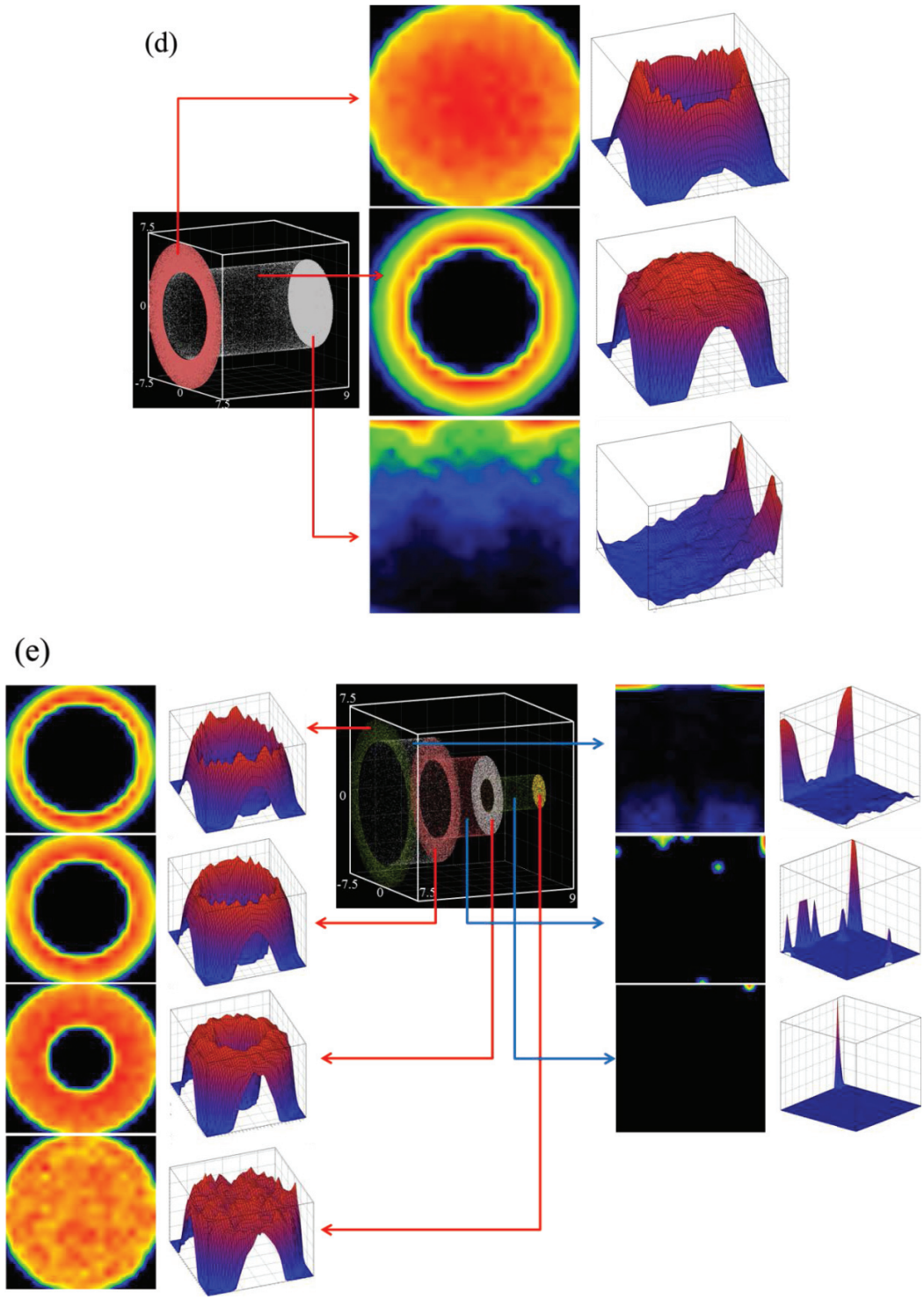

Fig 8 (b) ~ (e). The contour of flux intensity – (b) Model 1, (c) Model 2, (d) Model 3, and (e) Model 4

5. Discussion

The simulation of flux distribution on the 5 suggested models was calculated by the optical simulation code Soltrace. Each model has a different shape, exposure area, and volume. The calculated results describe the heat flux intensity on separated surfaces. Table 4. shows the peak heat flux intensity and average heat flux at each separated zone in the 5 device models.

Table 4. Input power, peak heat flux, and average heat flux on the separated zones of the 5 device models.

Input Power (kW)		Flat disk	Model 1	Model 2	Model 3	Model 4
		23.2	26.1	27.4	23.3	26.3
D. A. 1	Peak flux	2,424.5	1,358.5	2,109.2	1,857.0	1,116.2
	Average flux	1,031.8	375.2	622.0	493.4	271.2
D. A. 2	Peak flux		252.1	270.6	218.4	2,561.9
	Average flux		15.8	28.5	37.7	874.6
D. A. 3	Peak flux		3,310.9	3,326.5	2,096.6	3,137.8
	Average flux		1,739.3	1,971.9	1,291.6	1,632.5
D. A. 4	Peak flux					2,868.2
	Average flux					1,548.2

D. A. means the direct irradiated area.

The input power was calculated for each device model. The range of input power was 23.2 kW to 27.4 kW for the simulation. The separated direct irradiated zone (D. A.) is different among all 5 models. In the case of the flat disk type, there is only one zone. On the other hand, the models 1, 2 and 3 have a tripartite zone detailing the results: the ring zone at the aperture region of the device; the cylinder wall zone through the device depth; and the disk zone at the end point of the device. The D.A 1 is the results of ring zone, D.A 2 is the cylinder wall zone, and the D.A. 3 is the disk zone. In the case of model 4, named conical shape, 7 separate zones describe its heat flux intensity. As shown in Table 4, the heat flux intensity of the cylinder wall from models 1, 2, and 3 are considerably weaker than those pertaining to the ring zone. The results of the cylinder wall zone of model 4 are therefore excluded from the table. Thus the values of D. A. 1 to D.A. 4 in the model 4 column show only the results of the ring zone (D. A. 1 to D. A. 3) and the disk zone (D. A. 4).

In models 1, 2 and 3, the heat flux intensity of separated zone reveal an increasing tendency form D.A. 1 to D. A. 3 excepting D. A. 2 (the cylinder wall zone). This means that some of the concentrated sun rays hits the aperture of devices, while most of the sun rays are delivered to the disk zone (D. A. 3) through the device depth direction.

The largest peak heat flux was obtained from the case of model 1 D. A. 3 (disk zone) and the peak value was 3310.9 kW/m^2 whereas the largest average heat flux intensity was calculated to 1971.9 kW/m^2 from the case of model 2 D. A. 3 (disk zone).

The interesting points of the results obtained by the five model calculation is that the heat flux intensity of the cylinder wall zone (D. A. 2) shows very weak values compared to the ring zone and disk zone (D. A. 1 and D. A. 2). These findings reveal that concentrated sun rays have a directional characteristic, namely, predominant heat flux intensity on the normal direction on dish and perpendicular direction heat flux intensity at very low value. It means that to obtain uniform heat flux distributions on the device, normal directional surfaces have to be considered more carefully than perpendicularly directed surfaces.

6. Conclusion

By calculating the heat flux intensity of the above – mentioned devices, the flux distributions from the solar furnace system were simulated. The results clearly establish that concentrated sun rays have predominant heat flux

intensity at a normal direction instead of perpendicular direction. These results will be assessed in coming solar demonstrations that include a new solar reactor design for the KIER solar furnace.

References

[1] T. Kodama, N. Gokon. "Thermochemical cycles for high-temperature solar hydrogen production." *Chemical Reviews* **107.10**, 2007, pp. 4048-4077.

[2] Y. Tamaura et al. "Solar hydrogen production by using ferrites." *Solar Energy* **65**.1**,**1999, pp. 55-57.

[3] Furler, Philipp, et al. "Solar thermochemical CO2 splitting utilizing a reticulated porous ceria redox system." *Energy & Fuels* **26.11**, 2012, pp. 7051-7059.

[4] Abanades, et al. "Thermochemical hydrogen production from a two-step solar-driven water-splitting cycle based on cerium oxides." *Solar Energy* **80**.**12**, 2006, pp.1611-1623.

[5] T. Kodama, N. Gokon. "Two-step thermochemical cycles for high-temperature solar hydrogen production." *Advances in Science and Technology* **72**, 2011, pp. 119-128.

[6] Chueh et al. "A thermochemical study of ceria: exploiting an old material for new modes of energy conversion and CO_2 mitigation." *Philosophical Transactions of the Royal Society A: Mathematical, Physical and Engineering Sciences* **368**.1923, 2010, pp.3269-3294.

[7] Neises-von Puttkamer, M., Simon, H., Schmücker, M., Roeb, M., Sattler, C., Pitz-Paal R., Material Analysis of Coated Siliconized Silicon Carbide (SiSiC) Honeycomb Structures for Thermochemical Hydrogen Production. Materials 2013, 6, 421-436

[8] Kodama, T., Hasegawa, T., Nagasaki, A., Gokon, N., Reactive Fe-YSZ coated foam devices for solar two-step water splitting. Proceedings of the ASME Solar Energy Division, Energy Sustainability, 2007, *(ES2007)*, Long Beach, California, USA (ISBN: 0-7918-3798-X).

[9] Gokon, N., Hasegawa, T., Takahashi S., and Kodama, T., Thermochemical two-step water splitting for hydrogen production using Fe-YSZ particles and a ceramic foam device. Energy, 2008,**33**[9], pp.1407-1416.

[10] Gokon, N., Murayama, H., Nagasaki, A., and Kodama, T., Thermochemical two-step water splitting cycles by monoclinic ZrO_2-supported $NiFe_2O_4$ and Fe_3O_4 powders and ceramic foam devices. Solar Energy, 2009, **83**, pp.527-537.

[11] Kodama, T., Hasegawa, T., Nagasaki, A., Gokon, N., A reactive Fe-YSZ coated foam devices for solar two-step water splitting. J. Sol. Energy Engineering 2009, vol. 131, pp.021008-1-021008-7.

[12] T. Kodama, N. Gokon, J. Umeda, K. Sakai, and T. Seo,. THERMOCHEMICAL TWO-STEP WATER SPLITTING BY ZIRCONIA SUPPORTED FERRITES AND ITS FOAM DEVICE FOR SOLAR DEMONSTRATON. SolarPACES 2009, Berlin, Germany, September 15-18 2009.

[13] Abanades, et al. "Design and simulation of a solar chemical reactor for the thermal reduction of metal oxides: case study of zinc oxide dissociation." *Chemical Engineering Science* **62.22**, 2007, pp. 6323-6333.

[14] Shuai, Yong, Xin-Lin Xia, and He-Ping Tan. "Numerical study of radiation characteristics in a dish solar collector system." *Journal of Solar Energy Engineering* **130.2,** 2008, pp. 021001.

[15] Wendelin, Tim. "SolTRACE: a new optical modeling tool for concentrating solar optics." *ASME 2003 International Solar Energy Conference*. American Society of Mechanical Engineers, 2003.

[16] H.J. Lee, SolarPACES Symposium; 2012.

[17] K.K. Chai, The Korean Solar Energy Society Conference; 2011.

[18] H.J. Lee, Solar energy, 86.5, 1576-1585; 2012